CHAPTER 5

Polymer Network Dynamics during Electrospinning: Random Walk Simulation

ISRAEL GREENFELD* AND EYAL ZUSSMAN

Department of Mechanical Engineering, Technion – Israel Institute of Technology, Haifa 32000, Israel
*Email: green_is@netvision.net.il

5.1 Introduction

Electrospinning is an extensional flow characterized by high strain rates of order 10^3 s^{-1}.[1–7] Such stretching can potentially improve the structural order within as-spun nanofibers and enhance their mechanical properties such as elastic modulus and strength.[8–14] At the same time, rapid solvent evaporation during electrospinning can lead to increased polymer concentrations at the jet boundary,[15–18] sometimes forming a solid skin and a heterogeneous, porous structure.[11,17,19] Hence, study of electrospinning polymer solution jets, particularly of the evolution of the polymer entangled network during electrospinning,[11] is of interest in clarifying the microstructure of as-spun nanofibers.

Theoretical modeling of the polymer network dynamics during electrospinning, combined with random walk simulations of polymer chain conformations, showed substantial network stretching that occurs during the initial stage of electrospinning, several millimeters from the jet start.[11] That stretching is accompanied by lateral contraction of the network, resulting in a dense and compact polymer matrix at the jet core, verified by fast X-ray

RSC Polymer Chemistry Series No. 14
Electrospinning: Principles, Practice and Possibilities
Edited by Geoffrey R. Mitchell

Published by the Royal Society of Chemistry, www.rsc.org

phase-contrast imaging of electrospinning jets.[20] Furthermore, scanning near-field optical microscopy (SNOM) of fully solidified electrospun nanofibers confirmed that the fiber core has a higher density than its boundary, as well as a preferred molecular orientation in the direction of the fiber axis.[21]

The adaptation and application of polymer random walk simulation to an extensional flow, specifically to electrospinning of semi-dilute polymer solutions, provides a powerful tool for the analysis of the polymer network dynamics under various flow conditions and polymer conformations. In the following text, the random walk concept is explained, its theoretical basis and simulation tool are described, two types of single chain extension are demonstrated (chain under tension and chain in a flow field), and finally the polymer network dynamics in a flow field is simulated and discussed.[22] Experimental evidence supporting the simulation results is briefly presented.

5.2 Random Walk Simulation of Polymer Chains

5.2.1 Background

A flexible polymer chain in equilibrium state, having a degree of polymerization N, can be described by N successive steps of fixed length a, where a step represents a single monomer (or Kuhn segment). Each step is independent and has the same probability to move in any of the six Cartesian directions. Such a chain is called a freely-jointed chain, meaning that above the scale of a Kuhn segment the correlation between adjacent segments is lost (*i.e.,* restrictions due to bond angles and steric hindrance occur only below that scale), and the segments are free to move in any direction. Random walk on a Cartesian lattice can describe each possible chain conformation of a freely-jointed long chain. The three-dimensional end-to-end distance $\vec{R}$ of such a free ideal chain has a Gaussian distribution:[23]

$$P(\vec{R},N)=\left(\frac{3}{2\pi R_0^2}\right)^{3/2}\exp\left(-\frac{3\vec{R}^2}{2R_0^2}\right)\quad\text{where } R_0^2=a^2N. \tag{5.1}$$

The distribution of each Cartesian component of $\vec{R}$ is normal, with mean at zero. The probability that the end-to-end distance $R=\mid\vec{R}\mid$ will be within a spherical shell of radius R and thickness dR is[23]

$$P(R,N)4\pi R^2\mathrm{d}R=\left(\frac{3}{2\pi R_0^2}\right)^{3/2}\exp\left(-\frac{3R^2}{2R_0^2}\right)4\pi R^2\mathrm{d}R. \tag{5.2}$$

Examples of free chain simulations are shown in Figures 5.1 and 5.2.

A RW (random walk) simulation consists of generating a large enough sample of individual walks, each constructed from N successive unit-steps, and then generating a distribution of a chosen parameter (end-to-end

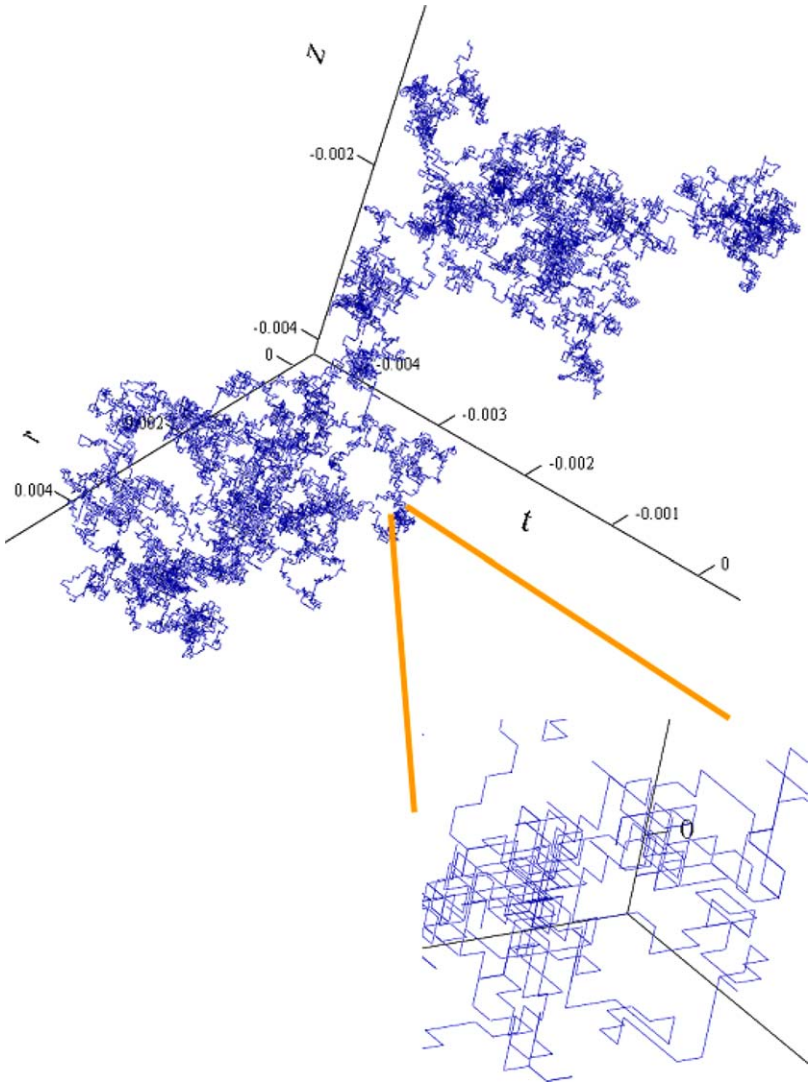

Figure 5.1 Example of random walk simulation of a single free flexible chain on a Cartesian lattice, with $N = 2000$ monomers (rigid chain elements).

distance, segmental orientation, *etc.*) from the complete sample, and finding the statistical moments and other characteristic features of the distribution.

Random walk simulation of a polymer chain or a network in a solution can be an effective tool for describing the polymer conformation, especially when the theoretical solution is too complex, when visualization of the behavior of an individual chain is desired, or when applying complex boundary constraints and potential fields (*e.g.,* a non-uniform flow). Under the effects of boundary or strong extensional flow, the statistical conformation of

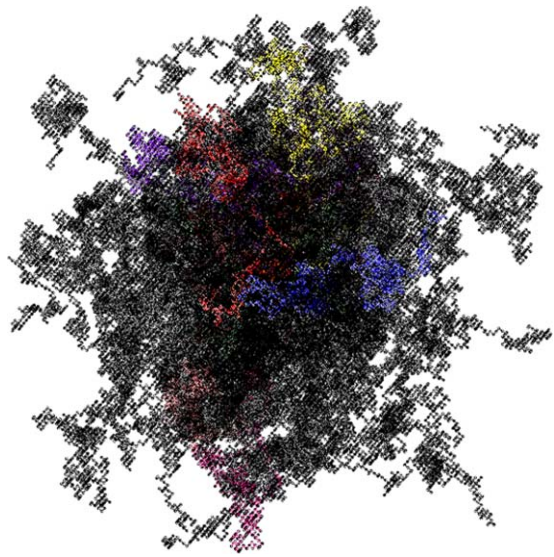

Figure 5.2 Example of random walk simulation of 100 free flexible chains on a Cartesian lattice. All of the chains start from the same point, and each chain contains $N = 2000$ monomers.

polymer chains is not Gaussian. The RW simulation tool presented here was developed and used extensively to investigate the conformation of the polymer chains and network during electrospinning, under varying process variables such as molar mass, flow strain rate, and solution viscosity.[11,22]

Although RW is efficient in providing the complete conformational statistics of a chain, the applicability of the method requires some simplifying assumptions on chain type, walk type, and monomers connectivity. The RW model used here is non self-avoiding, meaning that monomers in the chain are allowed to overlap (*i.e.,* occupy the same lattice position). The simulated chains are therefore ideal and not real, resulting in tighter chain conformations. However, this difference is of second order compared to the effects of external forces on the conformation. Moreover, for the concentrated solutions used in electrospinning, an ideal chain model is a good estimate, since in dense systems the repulsive forces between distant monomers in a chain are screened by repulsive forces from neighboring monomers of other chains.[23,24]

An important concern is whether random walk adequately represents the monomers connectivity in a chain under tension. Each random walk step is completely independent of the preceding and succeeding steps, and therefore can be described as a Brownian motion of a single particle. However, under external forces, free Brownian motion is not applicable, since monomers apply tension forces on their linked neighbors, and therefore their motion is not independent. The approach used here is to define an effective potential field that represents the external forces, similar to the

potential arising from hydrodynamic friction suggested by Kramers,[25] and to calculate the RW stepping probabilities from the potential gradient. This approach is shown to be valid in Section 5.3.1.

5.2.2 Theoretical Basis

A monomer in a linear chain or chain section, in the presence of an effective potential field U, experiences a force $F = -\nabla U$, where ∇U is the potential gradient. This effective potential may arise from an external force acting at the chain ends, which propagates evenly along the chain, or from a local force acting directly on monomers such as a hydrodynamic force, or from a combination of both force types (Figure 5.3).

From statistical mechanics it is known that, if a system in equilibrium can be in any one of several states, the probability that the system will be in a state having a potential U is $e^{-U/(k_B T)}/Q$, where T is the temperature and k_B is the Boltzmann constant.[26] The partition function Q is determined so that the sum of the probabilities of all the possible states equals 1. In terms of a RW on a Cartesian lattice, the probability ${P_x}^{\pm}$, that the system will make a step a in any of the 6 possible directions, is defined as ${P_x}^{\pm} \equiv {P_x}^{\pm}(x \to x \pm a)$, where $x = z$, ρ, φ are the three Cartesian axes. Therefore

$$P_x^{\pm} = \frac{1}{Q}\exp\left(-\frac{U_{x\pm a} - U_x}{k_B T}\right) = \frac{1}{Q}\exp\left(\mp\frac{\nabla U_x a}{k_B T}\right), \tag{5.3}$$

where ∇U_x is the potential gradient in the direction x. In correspondence to an electrospinning jet, z is coincident with the jet main axis, while ρ and φ are two radial mutually perpendicular axes. The sum of the probabilities of the 6 possible states of the system should be a unity

$$\sum_x {P_x}^{\pm} = \sum_x (P_x^{+} + P_x^{-}) = \frac{2}{Q}\sum_x \cosh\left(\frac{\nabla U_x a}{k_B T}\right) = 1, \tag{5.4}$$

from which Q can be derived. Defining a normalized force (using $F = -\nabla U$)

$$f = \frac{Fa}{k_B T} = -\frac{\nabla U a}{k_B T}, \tag{5.5}$$

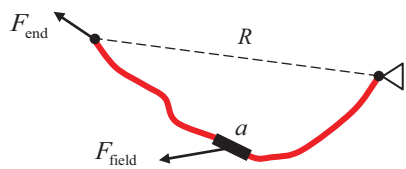

Figure 5.3 The general case of forces acting on a chain or a chain section. An external force F_{end} acts at the chain end and, in addition, a potential field applies a force F_{field} on each monomer a.

and substituting into eqn (5.3), we obtain the probabilities for a random walk step under a force f[11]

$$P_x^{\pm}(z,\rho,\varphi) = \frac{\exp\left[\pm f_x(z,\rho,\varphi)\right]}{2\sum_x \cosh[f_x(z,\rho,\varphi)]},\ x = z,\rho,\varphi. \tag{5.6}$$

Since the potential is a function of the three-dimensional position (z, ρ, φ), the force acting on a monomer, and its related stepping probabilities, are written as functions of the position.

The three force functions, (f_z, f_ρ, f_φ), can be any functions of the 3D position of the current monomer (z, ρ, φ). For example, using quadratic functions of the position, the force functions could be

$$\begin{aligned} f_z(z) &= A_{z,0} + A_{z,1}z + A_{z,2}z^2 \\ f_\rho(\rho,z) &= A_{\rho,0} + A_{\rho,1}\rho + A_{\rho,2}\rho z \\ f_\varphi(\varphi,z) &= A_{\varphi,0} + A_{\varphi,1}\varphi + A_{\varphi,2}\varphi z, \end{aligned} \tag{5.7}$$

where $A_{x,i}$ are constants. These functions are suitable (with adjustments) for describing the cases of interest, particularly the force field of the electrospinning jet (Section 5.4), in which the corresponding constants of the functions f_ρ and f_φ are equal. The constants $A_{x,0}$ represent forces acting at the chain ends, whereas the other terms represent a force field which varies as a function of the monomer position. The field force in the positive direction of z grows quadratically with z, while the radial field forces, which are acting toward the jet center, grow linearly with z and diminish toward the jet center. Consequently, all the constants should be positive, except for the prefactors of ρ and φ, which should be negative.

The random walk 3D simulation based on this concept was implemented in a computer program described in Section 5.6.1.

5.3 Single Chain

5.3.1 Chain under Tension

The modeling of this case is strongly related to the dynamics of the polymer network during electrospinning since, as will be explained in Section 5.4 of this chapter, the dominant force acting on a subchain entangled in a network is the extension force exerted at its ends by the linked subchains.

A longitudinal (normalized) force f_z, acting at the chain ends, propagates from one monomer to another, so that the force on each monomer is equal to f_z. Since the transversal forces f_ρ and f_φ are zero, the probability that the monomer will step in the longitudinal positive and negative directions is [eqn (5.6)]

$$P_z^{\pm} = \frac{\exp(\pm f_z)}{2[\cosh f_z + 2]}. \tag{5.8}$$

Similarly, the probability to step in one of the transversal positive and negative directions is

$$P_{\rho}^{\pm} = P_{\varphi}^{\pm} = \frac{1}{2[\cosh f_z + 2]}. \tag{5.9}$$

Since in this case the stepping probabilities are the same for all the N monomers in the chain, it is possible to derive an analytical solution for the chain mean end-to-end distance, R, that results from the end force

$$R_x = R_{\max}(P_x{}^{+} - P_x{}^{-}), \quad x = z,\ \rho,\ \varphi, \tag{5.10}$$

where $R_{\max} = aN$. Substituting the stepping probabilities from eqn (5.8) and (5.9), the mean longitudinal distance is

$$\frac{R_z}{R_{\max}} = \frac{\sinh(f_z)}{\cosh(f_z) + 2}, \tag{5.11}$$

while the transversal distances are $R_{\rho} = R_{\varphi} = 0$.

An example of a RW simulation of the extension of a freely-jointed chain under several values of the end force is shown in Figure 5.4. The force-elongation relationship of a freely-jointed chain, obtained by the RW simulation, is shown in Figure 5.5, and is compared with the Gaussian $[R_z/R_{\max} = f_z/3]$,[24] Langevin $[R_z/R_{\max} = [\coth(f_z) - 1/f_z]]$,[23] and Analytic [eqn (5.11)] solutions. The Gaussian solution represents Hooke's law, and is valid only for small elongations, whereas the Langevin and RW solutions, both saturate at elongations approaching the extension limit of the chain.

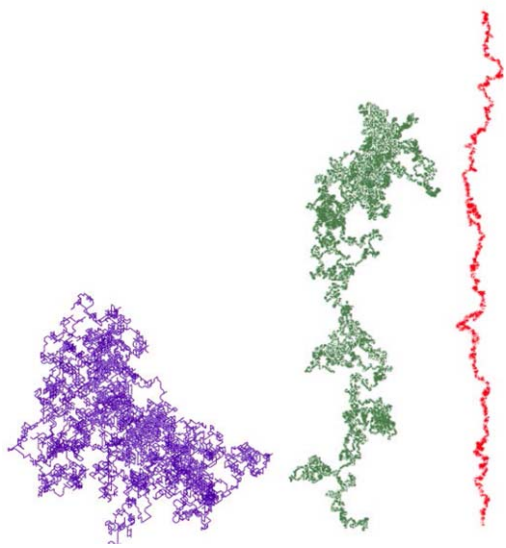

Figure 5.4 Random walk simulation of a freely-jointed chain with $N = 10\,000$ monomers. The stretching end force, f_z, is (from left) 0 (free state), 0.05, and 0.3.

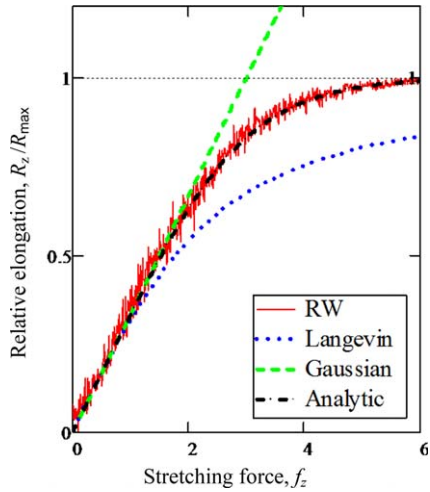

Figure 5.5 Force-elongation relationship of a freely-jointed chain. Comparison of the mean elongation of random walk (RW) simulation of 10 chains, each with $N = 30$, to Langevin, Gaussian, and Analytic solutions.

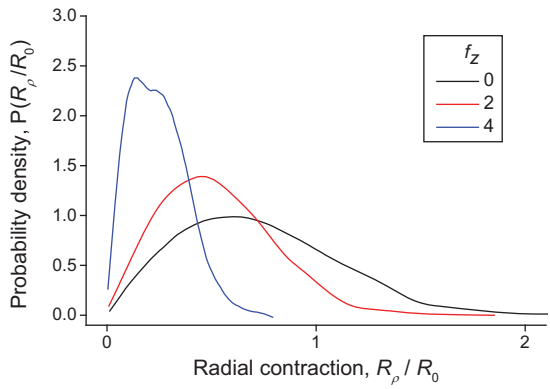

Figure 5.6 Probability density of the radial mean-square end-to-end distances, for three values of the stretching end force f_z (from left): 4, 2, and 0. $I = 1000$ simulated chains, each with $N = 500$ monomers.

The redistribution of stepping probabilities during application of a longitudinal extension (see example in Figure 5.20), results in lateral contraction of the chain, as seen in the narrowing of the distribution of the chain mean-square end-to-end radial distance in Figure 5.6 when the tension force is increased. The mean-square radial distance is calculated from the simulated distribution [the function $R(I, N)$ in Figure 5.22], and is normalized by the mean-square end-to-end distance of a free chain, $R_0 = aN^{1/2}$.

$$\frac{R_\rho}{R_0} = \frac{|\,R_\rho\,|}{N^{1/2}}. \tag{5.12}$$

Also, as a result of stretching, the alignment of chain segments with respect to the z axis increases. The orientation parameter O is averaged over the complete contour length of the chain

$$O = \frac{3}{2}\langle \cos^2\theta \rangle - \frac{1}{2}, \quad \langle \cos^2\theta \rangle = \frac{1}{N-2m+1}\sum_{n=m}^{N-m}\left[\frac{|\, z_{n+m} - z_{n-m}\,|}{|\, \vec{R}_{n+m} - \vec{R}_{n-m}\,|}\right]^2, \quad (5.13)$$

where θ is the angle between the segment's end-to-end direction and the z axis, and $2m + 1$ is the number of monomers in the segment. The result is then averaged over a sample of chains to reduce noise. As expected, the orientation increases when the force is higher (Figure 5.7). Obviously, the orientation depends on the size of the selected segment: when too short, the Cartesian lattice can introduce an error, whereas, when too long, the orientation gradually drops to 0.

5.3.2 Free Chain in a Flow Field

A single chain in a flow field is not representative of the dynamic behavior of a polymer network during electrospinning. However, this problem was investigated analytically by de Gennes[24,27] and others, and therefore it is interesting to study it with a different tool. Moreover, the extension of the chain in this case is not uniform, unlike the case of a chain under tension at its ends (described in the previous section), but varies along its contour, somewhat analogous to the conformation of a polymer network along an electrospinning jet.

A single chain in an extensional flow field experiences field forces acting directly on its monomers. The force on a single monomer of size a can be estimated by Stokes law

$$F = k_G a \eta_s v, \quad (5.14)$$

where η_s is the solvent viscosity, v is the velocity difference between the monomer and the solvent, and k_G is a dimensionless geometrical factor of

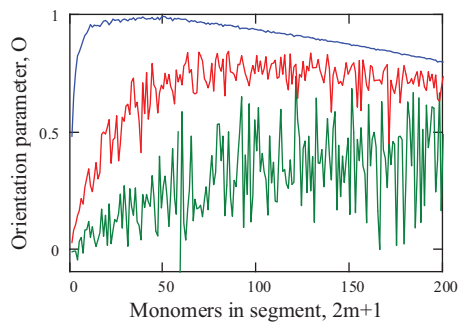

Figure 5.7 Segmental orientation as a function of the number of monomers in a segment, for three values of the stretching end force f_z (from top): 2, 0.5, and 0.2. The number of monomers in a chain is $N = 1000$.

order 1 that depends on the monomer's shape. Assuming that the center of the sum of forces is moving at the velocity of the jet, the origin of a Cartesian coordinate system $x=(z,\ \rho,\ \varphi)$ can be attached to the force center, with z pointing toward the direction of the flow. Within the small scale of a single chain, the velocity gradient can be considered constant, and therefore the force center is located approximately at the chain center; however, this condition is not necessary, so long as the location of the force center on the chain is known. The velocity v is then the jet velocity with respect to the moving force center. Writing the velocity in units of step per s instead of nm s^{-1} (in common polymers 1 step has the scale of 1 nm), and normalizing the force as in eqn (5.5)

$$f=\frac{Fa}{k_BT}\cong\frac{k_Ga^3\eta_s}{k_BT}v\cong\tau_0 v, \tag{5.15}$$

where $\tau_0\approx\eta_s a^3/(k_BT)$ is the monomer's relaxation time.[23]

In the case of a constant velocity gradient s in the z direction (remembering that z is referenced to the force center), and no gradient in the perpendicular directions

$$f_z\cong s\tau_0 z. \tag{5.16}$$

The dimensionless parameter $s\tau_0$ is the force field coefficient $A_{z,1}$, used in the force functions of eqn (5.7). Due to symmetry with respect to the chain center, which coincides in this case with the force center, the random walk is run for half the chain. Note that the force can be rewritten in the form $f_z\approx s\tau\bar{z}/N$, where $\tau\approx\tau_0N^{3/2}$ is the chain relaxation time,[23] and $\bar{z}=(z/N^{1/2})$ is the relative position. This form incorporates the familiar $s\tau$ term, used by de Gennes to express the condition for coil stretch transition.[24]

The results of the corresponding RW simulation provide a striking resemblance to the analytic solution by de Gennes. The distribution $P(R/R_0)$ of the chain's end-to-end distance $R=|\vec{R}|$ in Figure 5.8 shows that, when gradually increasing $s\tau_0$, the end-to-end distance of the chain transitions from small elongation to very large elongation, with an intermediate widely spread bimodal distribution (inset). The entropy of the chain is given by $S=k_B\ln(\Omega)=\text{const}+k_B\ln[P(r)]$, where $P(r)$ is the probability of the extension r, and Ω is the number of possible coil configurations for a given extension vector r, proportional to $P(r)$. The total Helmholtz free energy (elastic + friction) of the chain is calculated by $F_{tot}=U-TS$, where U is the chain constant internal energy, independent of chain conformation because an ideal chain assumes no interaction energy between distant monomers. Thus,

$$\frac{F_{tot}}{k_BT}=\text{const}-\ln\left[\frac{P(R/R_0)}{4\pi(R/R_0)^2}\right], \tag{5.17}$$

where the term $4\pi(R/R_0)^2$ is inserted in order to convert the distribution from the 1D form of eqn (5.2) to the 3D form of eqn (5.1). The energy is depicted in

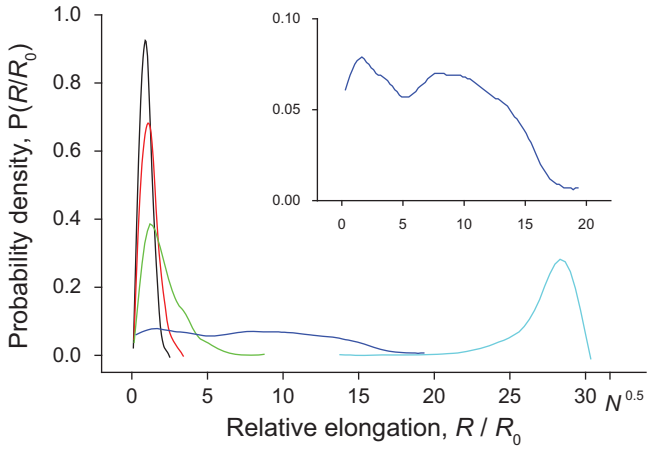

Figure 5.8 Probability density of relative end-to-end distances R/R_0 of a polymer coil in an extensional flow with a constant gradient. $I = 1000$ simulated chains, each with $N = 1000$ monomers. The field force is $s\tau_0 z$, where $s\tau_0$ is (from left): 0, 0.003, 0.006, 0.012, and 0.063. The inset ($s\tau_0 = 0.012$) shows a transitional bimodal density.

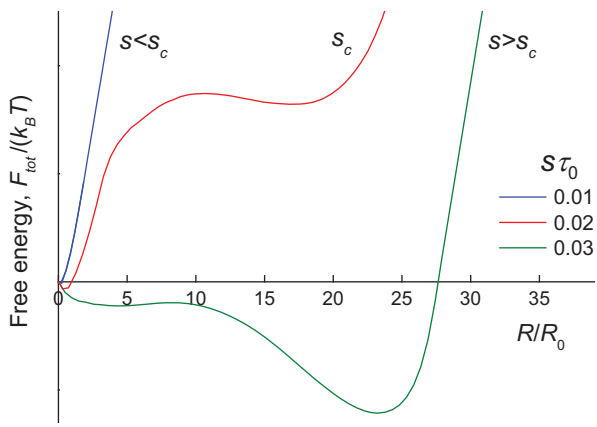

Figure 5.9 Free energy versus the relative elongation of chains under a field force $s\tau_0 z$ in an extensional flow with a constant gradient. Calculated for three values of $s\tau_0$ (from left): 0.01, 0.02, and 0.03. $N = 1000$ monomers.

Figure 5.9, in excellent agreement with de Gennes.[24] Below a critical gradient s_c, the elongation is Gaussian, while above it the curve corresponds to large elongation and has two energy minima, eventually converging to very large elongation.

The value of the critical gradient s_c, where coil stretch transition occurs, is seen in Figure 5.10 for three values of the degree of polymerization N. This plot was achieved by calculating the elongation distribution for each value of

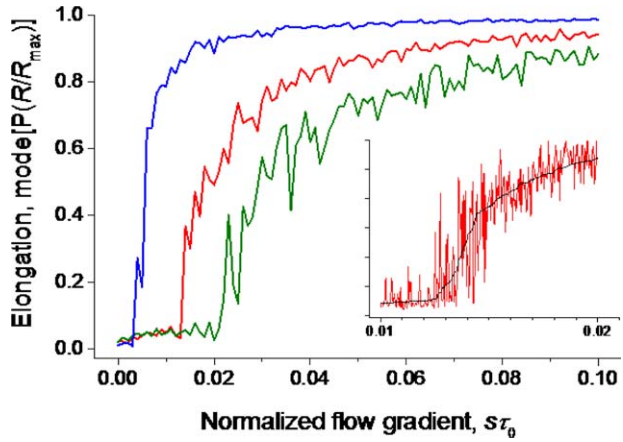

Figure 5.10 The distribution mode of the relative elongation R/R_{max} of a single polymer coil in an extensional flow with a constant gradient, *versus* the normalized flow gradient $s\tau_0$. The field force is $s\tau_0\, z$. The value of N is (from left): 5000, 1000, and 500 monomers. The inset magnifies the transitional zone of the case $N = 1000$.

$s\tau_0$, and detecting the peaks of the probability density, from which the statistical mode (most frequent value) of the elongation is inferred.

Below the transition point, the dependence of the elongation on s is low (Gaussian), whereas above it the dependence is initially steep and then, at very high gradients, it tapers off. Around the transition point, within a very small $s\tau_0$ range (*e.g.,* 0.013–0.014 for the case $N = 1000$), the elongation fluctuates between small and large values (inset). Additionally, when the chain is longer (higher N), the hydrodynamic friction becomes dominant over the elastic force, and the transition point occurs at a lower s, as shown by de Gennes. For $N = 5000$ monomers, the transition occurs at a very low gradient.

The conformation of a chain extended by such a force field is different from a chain under tension at its ends, described in the previous section. While a chain under tension has a uniform density along its contour (top view of Figure 5.11), a chain in a force field is denser around its center, where the force is low, and more extended farther from the center, where the force is high (bottom view).

5.4 Network in a Flow Field

5.4.1 Polymer System and Forces

Polymer in a semi-dilute solution forms an entangled network. In such a network, each chain segment between two adjacent topological links (*i.e.,* topological constraints), can be practically regarded as a subchain, with an end-to-end distance ξ, equivalent to the network mesh size (see illustration in Figure 5.12). When the jet strain rate is low, rapid relaxation of polymer

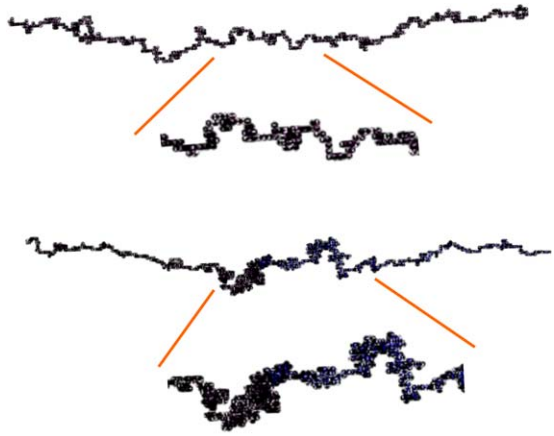

Figure 5.11 Examples of extended chains with $N = 1000$. The top view is a chain under tension at its ends. The bottom view is a chain under a force field, such as a flow with a constant strain rate in the direction of the chain's elongation.

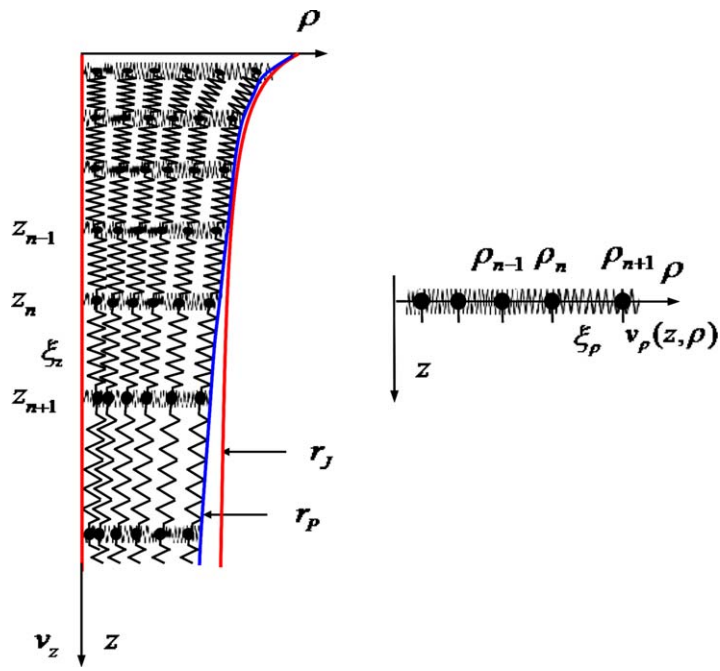

Figure 5.12 Illustration of polymer network stretching in an electrospinning jet, and definition of an effective 1D system describing the polymer network stretching in the axial direction z (left) and the radial direction ρ (right). r_J and r_P denote the jet and polymer network radii, respectively.
Adapted from ref. 11.

chains results in a viscous flow; however, at high strain rates, relaxation is not sufficiently fast and elasticity is dominant, making the elastic extension of subchains possible. When subchains approach full extension, they will tend to disentangle from the network, an effect ignored in the analysis presented here (entanglement loss is addressed in ref. 28).

Each subchain experiences an extensional force at its ends, exerted by the other subchains connected to the same topological links, and a local hydrodynamic force acting on each of the subchain's monomers by the solvent (Figure 5.13). Since the scale of a single subchain ($\sim$10 nm) is several orders of magnitude smaller than the scale of the electrospinning jet ($\sim$1 mm), the tension gradually builds up from subchain to subchain due to network connectivity, and becomes dominant over the hydrodynamic force. The subchain can therefore be treated as a single chain under tension, as in Section 5.3.

Subchains in a network at rest have an end-to-end distance ξ_0, caused by an effective stretching force [normalized as in eqn (5.5)] of scale[11]

$$f_0 = \tanh^{-1}\left(\frac{3a}{\xi_0}\right) \approx \frac{3a}{\xi_0} \approx \frac{3}{\sqrt{N_s}}, \tag{5.18}$$

using the Gaussian force-elongation relationship $f_0 = 3R_0/R_{max}$,[23] where $R_0 = \xi_0 = aN_s^{1/2}$, $R_{max} = aN_s$, and N_s is the number of monomers in the subchain. The first term was obtained from eqn (5.28) at jet start. For a given polymer volume concentration ϕ, $\xi_0 \cong a\phi^{-1}$ and $N_s \cong \phi^{-2}$ (ideal chain).

The force on a monomer in a flow field is $F = k_G a\eta v$ [eqn (5.14)], where η ($\eta > \eta_s$) is the effective viscosity of the dilute solution surrounding the monomer. In this, we assume that, although the solution as a whole is semi-dilute entangled, locally, the fluid around the monomer has a higher viscosity than that of the solvent, as a result of dissolved unentangled chains. Given a velocity gradient in the vicinity of a subchain n, ∇v_n, and the subchain end-to-end distance ξ_n, the average velocity increase along that

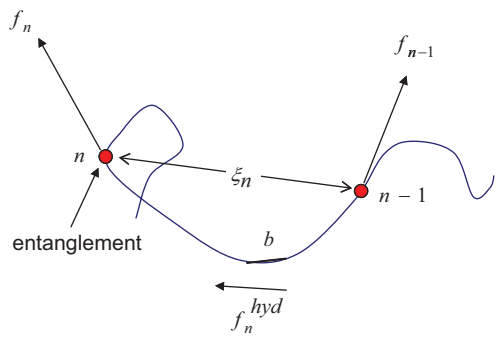

Figure 5.13 Tension forces and hydrodynamic forces acting on a subchain extending between two entanglements in a polymer network.

subchain is $\xi_n \nabla v_n$. Consequently, the hydrodynamic force grows with respect to the previous subchain, and the force on a monomer in that subchain is increased by[11]

$$\delta F_n \cong k_G a \eta \xi_n \nabla v_n. \tag{5.19}$$

This force is on average the same for all the monomers in the subchain, and is therefore equivalent to a tension force of the same scale applied at the subchain ends, as reasoned in Section 5.3. Writing the mesh size in unit steps instead of nm (1 step is $\sim$1 nm), and normalizing the force

$$\delta f_n = \frac{\delta F_n a}{k_B T} \cong \frac{k_G a^3 \eta}{k_B T} \xi_n \nabla v_n \cong \tau_0 \xi_n \nabla v_n, \tag{5.20}$$

where $\tau_0 \approx \eta a^3/(k_B T)$ is the monomer's relaxation time corresponding to the dilute viscosity η. Summing the friction forces over all the subchains in a desired direction, we obtain the total tension force acting on subchain n

$$f_n = \sum_{i=1}^{n} \delta f_i \cong \tau_0 \sum_{i=1}^{n} (\xi_i \nabla v_i) \cong \tau_0 (v_n - v_{n0}), \tag{5.21}$$

where v_n is the flow velocity around subchain n, and v_{n0} is the flow velocity at the origin of the first subchain, both in units of step per s. In view of the huge difference in scale between a subchain and the network, f_n and v_n can be written as continuous functions of the global position $x = (z, \rho, \varphi)$, or $f(z, \rho, \varphi)$ and $v(z, \rho, \varphi)$, in which the position corresponds to the subchain sequential number. Thus,

$$f_x \approx \tau_0 (v_x - v_{x0}), \tag{5.22}$$

where v_x and v_{x0} are the velocity and the initial velocity in the direction x, respectively. Adding the initial force of the network at rest from eqn (5.18), we obtain the total force on a monomer

$$f_x \approx f_0 + \tau_0 (v_x - v_{x0}). \tag{5.23}$$

The flow of the electrospinning jet has axial and radial velocity components. For a quadratic velocity profile, we use the form[11,29]

$$\begin{aligned} v_z &= v_0 (1 + kz)^2 \\ v_\rho &= -v_0 (1 + kz) k\rho, \end{aligned} \tag{5.24}$$

where v_0 is the jet initial velocity, k is a dimensionless parameter that determines the velocity gradient (of order 10^{-6}–10^{-4}), and the units of length and velocity are step and step per s, respectively. k depends on the process and material parameters, such as the jet initial velocity and radius, electrostatic field intensity, solution viscosity, and electric conductivity.[28,29] The corresponding jet radius (assuming volume conservation) is $r_J = r_0 (1 + kz)^{-1}$, where r_0 is the jet initial radius. The initial velocity in the axial direction is

taken at the jet start ($z = 0$), whereas the initial velocity in the radial direction is taken on the free surface of the jet ($\rho = r_J$), and therefore

$$\begin{aligned} v_{z0} &= v_0 \\ v_{\rho 0} &= -v_0 k r_0. \end{aligned} \tag{5.25}$$

Inserting the velocity expressions into eqn (5.23), we can now summarize the force functions for the random walk simulation (in unit steps) of an entangled subchain in a flow field, in a form similar to eqn (5.7):

$$\begin{aligned} f_z &= f_0 + \tau_0 v_0 k(2 + kz)z \\ f_\rho &= f_0 - \tau_0 v_0 k[r_0 - (1 + kz)\rho] \\ &= f_0 - \tau_0 v_0 k r_0 (1 - \rho / r_J). \end{aligned} \tag{5.26}$$

The forces in eqn (5.26) are specific to the quadratic velocity profile of eqn (5.24), but eqn (5.23) can be adapted to any velocity profile by the same logic. In view of the rotational symmetry in the radial direction, the same value of the force f_ρ is used for the force f_φ, an approximation that reduces the complexity of the simulation. Note that in the radial direction, the sign of the velocity was reversed since the network starts at the jet boundary and not at the center, and consequently, since $\rho < r_J$, the force due to the radial flow is negative (a compressive force). Also, the overall radial force should always be $f_\rho \geq 0$, since a negative value would mean stretching.

In the axial direction, the stretching force due to the flow rises quadratically with z and becomes much larger than f_0, and therefore $f_z \cong \tau_0 v_0 k^2 z^2$. In the radial direction, the compression force due to the flow decreases proportionally to the ratio between the local radius and the jet radius, and reaches a maximum magnitude of $\tau_0 v_0 k r_0$ at the jet center, independently of the position z. Typically, the order of magnitude of this compressive force is much lower than $f_0 \sim 10^{-1}$, and therefore it does not cause a significant compression with respect to the initial mesh size of the network. Hence, the dominant effect on the radial contraction of the network is that induced by the axial stretching force, which is many orders of magnitude higher than the radial compressive force (their ratio is of order $z/r_J \gg 1$). These effects are demonstrated in the simulation example shown in Figure 5.14. In fact, the influence of the radial compressive force is even lower, since the network radius becomes smaller than the jet radius as a result of stretching, and therefore the jet radius r_J in eqn (5.26) should be replaced by the smaller network radius r_P.

5.4.2 Network Dynamics

The network simulation procedure is described in Section 5.6.2. Typical results of a simulation run of a sequence of $\sim$9000 subchains in the axial direction are depicted in Figure 5.15, showing the evolution of the axial force and the axial and radial mesh sizes, as functions of the distance from the jet start. In this run, the radial compression force was ignored ($f_\rho = f_0$), allowing

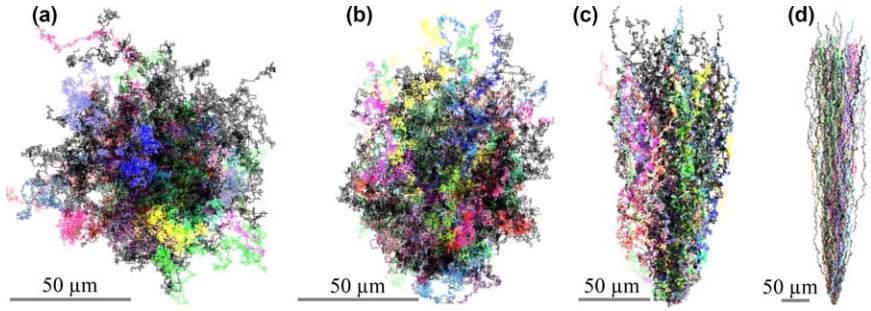

Figure 5.14 Example of subchains conformation generated by random walk, demonstrating the dominant effect of stretching over radial contraction. Each image consists of a sample of 100 subchains, starting from the same node. $N_s = 4000$. (a) Network at rest, $f_x = f_0$. (b) Maximal radial compression, $f_\rho = f_\phi = 0$. (c) Axial stretching, $f_z = 4f_0$. (d) Axial stretching, $f_z = 11f_0$.

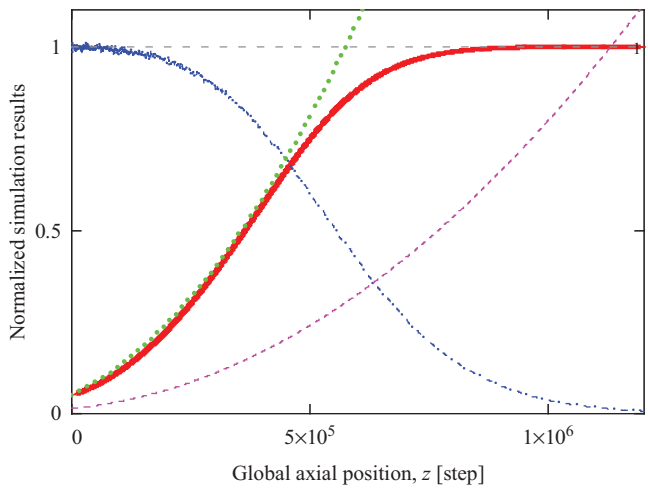

Figure 5.15 Simulation of a polymer network in an electrospinning jet, for a sequence of 8855 chains in the axial direction, using the force functions of eqn (5.26) with $f_\rho = f_\phi = f_0$. The plots are: ξ_z/N_s (solid), $\xi_\rho/(N_s/3)^{1/2}$ (dash-dot), $v_z/v_0/N_s^{1/2}$ (dot), and $f_z/f_0/70$ (dash). The simulation parameters are: $N_s = 400$ step (monomers), $\xi_0 = 20$ step, $f_0 = 0.15$, $v_0 = 2.6 \times 10^6$ step/s, $k = 6 \times 10^{-6}$, and $\tau_0 = 5.8 \times 10^{-8}$ s.

observation of the net effect of stretching on the radial mesh size, which indeed converges to zero around 10^6 steps from the jet start ($\sim$1 mm). At that position, the axial mesh size converges to the fully extended length of the subchain, and the axial force rises to $\sim 70f_0$. The parameter τ_0 was tuned so that at small elongations the axial mesh size will conform to that obtained by the affine stretching result of the theoretical modeling, represented by the dotted line.[11] Note that, unlike the theoretical model, which assumes linear

force-elongation (Gaussian) dependence, the stretching of a subchain modeled by RW is nonlinear and bounded by the subchain's fully extended length.

The overall simulated network is depicted in Figure 5.16(a), demonstrating the longitudinal extension and the simultaneous lateral contraction, resulting in a network radius smaller than the jet radius. An approximation for the network radius, when neglecting the radial compression force, can be obtained by[11]

$$r_P = r_J \frac{\xi_\rho}{\xi_0} \tag{5.27}$$

The conformation of a sequence of subchains is presented in Figure 5.16(b) and (c). Obviously, it is not likely that the network would have

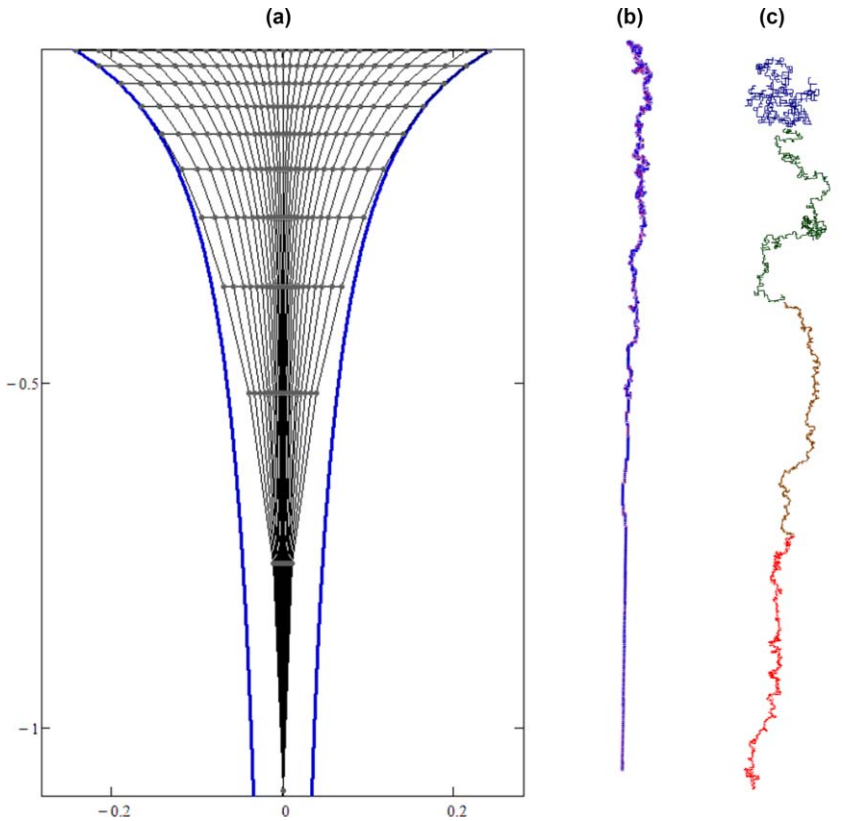

Figure 5.16 Conformation of the polymer network during electrospinning, simulated using the force functions of eqn (5.26), including radial compression. The conditions are as in Figure 5.15, with $r_0 = 2.5 \times 10^5$ step. (a) Network map of a jet section $\sim$1 mm long: line segments represent subchains and line crossings topological entanglements. Viewed density is diluted $\times$800 in each direction. The jet profile is depicted by the external lines. (b) A single vertical sequence of linked subchains along the z axis. (c) Same as (b), but with enlarged subchains (not to scale).

such a sharp boundary as depicted, but nevertheless the general phenomenon of network compacting should be expected. In this run, the radial compression force was included, and its effect can be noticed in the gradual growth of the radial density toward the jet center.

As already implied in the analysis of a single chain in a flow field (Section 5.3.2), the network simulation can be achieved by running a single "very long" chain of $\sim 10^7$ monomers, which represents a sequence of subchains in the axial direction. Shortly after the jet start, f_0 and v_0 in eqn (5.23) can be neglected, and the force function becomes analogous to that of a single chain in a flow field [eqn (5.15)], $f \cong \tau_0 v$. The force center is chosen at the jet start, where the relative velocity between the network and the solvent is zero, so that half of the chain extends in the direction $+z$, and the opposite half is imaginary. v is the jet velocity, and τ_0 is the monomer's relaxation time in the dilute fluid of viscosity η. Such a "long" chain is depicted in Figure 5.16(b). This analogy also implies the possibility of a network stretch transition, and the existence of two distinct energy equilibrium states and corresponding network stretching lengths; however, as pointed out in the single chain analysis, for a very long chain this transition occurs at a very low velocity gradient (see, for example, the left curve in Figure 5.10), and is therefore not expected during electrospinning.

5.4.3 Analytic Approximation

Using the same approach as for a single chain under tension (Section 5.3), the subchain mean end-to-end distance (mesh size), ξ, that results from the force functions (ignoring radial compression), is[11]

$$\frac{\xi_z}{\xi_{\max}} = \frac{\sinh[f_0 + \tau_0(v_z - v_0)]}{\cosh[f_0 + \tau_0(v_z - v_0)] + 2\cosh(f_0)},$$
$$\frac{\xi_\rho}{\xi_{\max}} = \frac{\sinh(f_0)}{\cosh[f_0 + \tau_0(v_z - v_0)] + 2\cosh(f_0)}. \tag{5.28}$$

These equations are in excellent agreement with the simulations (for example, the results shown in Figure 5.15). ξ_ρ can be derived from ξ_z by

$$\frac{\xi_\rho}{\xi_0} = \frac{3c\left[1 - (\xi_z/\xi_{\max})^2\right]}{2c + \left[1 + (4c^2 - 1)(\xi_z/\xi_{\max})^2\right]^{1/2}}, \quad c = \left(\frac{1 - 3a}{\xi_0}\right)^{-1/2}. \tag{5.29}$$

Shortly after the jet start, but before the network approaches full stretching ($f < 1$), the relative longitudinal elongation of a subchain can be approximated by

$$\frac{\xi_z}{\xi_0} \approx \frac{\xi_0 \tau_0 v_0}{3}\left(\frac{v_z}{v_0}\right). \tag{5.30}$$

The dimensionless prefactor $(1/3)\xi_0\tau_0 v_0$ (length in unit steps), or $(1/3)\xi_0 v_0 a\eta/(k_B T)$ (length in nm), determines the elongation of the network

with respect to that of the jet, and is of order $10^1 10_s^{-8} 10_{s^{-1}}^7 \sim 1$. Note the similarity between this prefactor and the dimensionless parameter α used in the theoretical modeling of the network in ref. 11 (they are the same if z_0 is substituted by a, and the inertia m is neglected), both of which determine the extent of affinity. In case $(1/3)\xi_0\tau_0 v_0 = 1$, the network elongation is affine, as found by the theoretical modeling. In case $(1/3)\xi_0\tau_0 v_0 \leq 1$, the network elongation is slower that the jet, and *vice versa*. Conversely, if affinity is assumed, the value of the monomer's relaxation time should be $\tau_0 = 3a^2/(\xi_0 v_0)$ (length in nm), and the corresponding effective viscosity should be $\eta \approx 3k_B T/(a\xi_0 v_0)$.

A criterion for the jet velocity v_s where subchains approach full stretching can be defined by substituting $\xi_z = N_s = {\xi_0}^2$ in eqn (5.30)

$$v_s \approx \frac{3}{\tau_0}, \tag{5.31}$$

in which unit steps are used. This expression converges to $v_s/v_0 \approx {N_s}^{1/2} \approx \phi^{-1}$ when affinity is assumed.[11]

In the case of a constant gradient $s = v_0 k$ in the z direction, the force in that direction is $f_z \approx s\tau_0 z \approx s\tau\bar{z}/N_s$ (ignoring f_0), where $\tau \approx \tau_0 {N_s}^{3/2}$ is the subchain relaxation time, and $\bar{z} = z/N_s^{1/2}$ is the relative position. This force is analogous to the force in the case of a single chain [eqn (5.16)]. The subchain end-to-end distance is $\xi_z \approx (1/3)N_s\tau_0 v_z \approx (1/3)s\tau\bar{z}$ (in unit steps).

5.5 Discussion and Conclusions

Extensional flow of a semi-dilute polymer solution under a high strain rate can cause substantial stretching of the polymer network. This effect was studied theoretically and experimentally, using the technique of electrospinning, a flow governed by high strain rate and rapid evaporation. Electrospun polymer nanofibers are of particular interest, in view of their small size and broad potential applications in engineering and life sciences. Their unique mechanical properties, such as a size-dependent elasticity which rises highly above that of bulk material, and the need to explain these properties, provide the incentive for investigating the polymer matrix conformation in electrospinning jets and in electrospun nanofibers.

Theoretical modeling and random walk simulations of the dynamic evolution of the entangled polymer network in an electrospinning jet predict substantial longitudinal stretching and radial contraction of the network, a transformation from an equilibrium state to an almost fully stretched state. The random walk simulation uses a beads-and-springs network model, with nonlinear entropic elasticity that allows large chain elongations. Affine network stretching is observed, and the conditions for affinity are defined. Subchains approach full extension not far (<1 mm) from the jet start, occurring when the jet velocity reaches a value inversely

proportional to the polymer volume concentration. The strong increase in the longitudinal mesh size is accompanied by a decrease in the radial mesh size as a result of the redistribution of the random walk stepping probabilities. The consequence is a lateral contraction of the network toward the jet center, proportional to the decrease in the subchains radial mesh size.

The transformation of subchains from a coil-like equilibrium state into a stretched state occurs as a continuous crossover, and no phase transition is observed, in contrast to the well-known coil stretch transition in unentangled free chains. The dominant local force on a subchain is the elastic force arising from the action of the topologically linked subchains, whereas the local hydrodynamic forces, whose accumulation along the network gives rise to the global elastic stretching, are negligible. There exists an analogy between a vertical sequence of linked subchains in a network and a very long free chain, implying the possibility of network stretch transition at low jet strain rates. However, under such conditions, the flow will be dominated by viscosity and network relaxation rather than elasticity, and therefore such transition is not expected in electrospinning. Stretching is uniform within the scale of a single subchain, while within the scale of the network it is nonuniform in a similar fashion to a single chain past the coil stretch transition condition.

The simulated predictions were supported by experimental evidence obtained from fast X-ray phase-contrast imaging of electrospinning jets (Figure 5.17): the polymer concentration at the jet center increased, with a

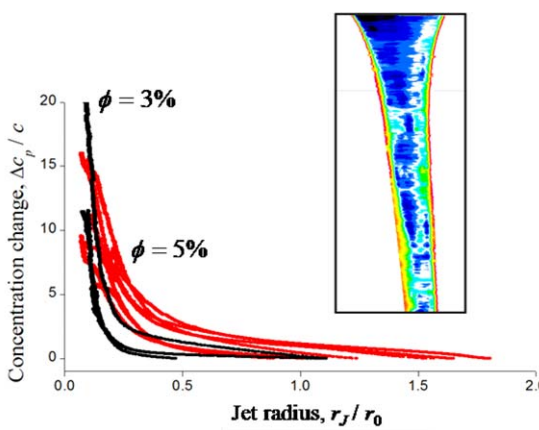

Figure 5.17 X-ray absorption measurements of electrospinning jets of PEO dissolved in water at 3% and 5% volume concentrations. Absorption coefficient map indicating an increase in polymer concentration at the jet core (right). Relative polymer concentration change at the jet center *vs.* relative jet radius (left).
Adapted from ref. 20.

distinct crossover that may indicate that the maximal stretching and compacting of the network was reached, occurring at a jet radius reduction ratio of only 4 : 1, close to the jet start. Further experimental support was obtained by scanning near field optical microscopy (SNOM) of electrospun conjugated optically active polymer nanofibers: a dense elongated molecular conformation was revealed, with a rise in the elastic modulus at the fiber core (Figure 5.18), confirming that the stretched and condensed structure remains after jet solidification.

The validity of the network modeling is restricted to the initial stage of the jet (first few millimeters), where elastic elongation is still possible, and therefore the model does not describe the final state of the polymer matrix in electrospun nanofibers. Additional processes, such as rapid evaporation and entanglement loss, which can result in chain relaxation, are not accounted for in the model (the effects of entanglement loss are analyzed in ref. 28). Nevertheless, the results strongly indicate non-equilibrium, ordered nanostructures that could remain in the nanofibers after solidification, structures which may set a new internal scale, and affect the nanofiber mechanical properties through confinement.

The random walk simulation, developed specifically for this investigation, provides a flexible and effective tool for analysis and visualization of polymer networks and individual chains in high strain rate flows. The tool was used extensively to investigate the conformation of the polymer chains and the network during electrospinning, under varying process variables, such as molar mass, flow strain rate, and solution viscosity. It is shown that, although several simplifications were applied in the simulation, the use of an

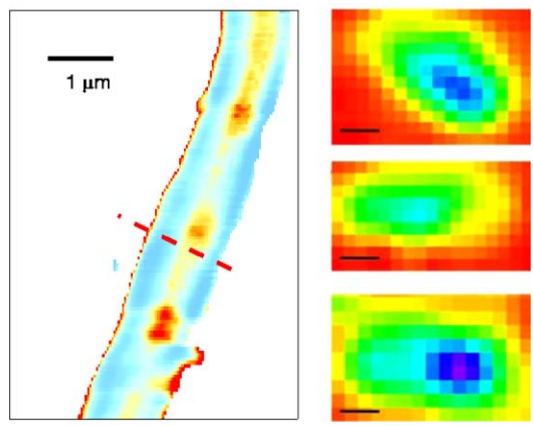

Figure 5.18 Optical and mechanical measurements of MEH-PPV nanofibers. Optical absorption SNOM map indicating higher polymer density at the fiber core (left). Young's modulus AFM maps of fiber cross-sections indicating increased modulus at the fiber core (right).
Adapted from ref. 21.

effective potential field induced by the flow represents well the physics of the polymer chains.

5.6 Appendix: Random Walk Simulation Tool

5.6.1 Program and Examples

The 3D random walk simulation was implemented in a program written in Mathcad. The core engine of the program consists of a stepping probability function and a stepping function. The simulation uses the uniform randomization function of Mathcad, and is dimensionless. Unit steps are used to represent monomers, but since for a given polymer the monomer size a is constant (of order 1 nm), the real dimensions of the chain can be restored without losing generality. Similarly, the force is dimensionless, as defined for eqn (5.5) and (5.6).

The stepping probability function, $P(z, \rho, \varphi)$ (Figure 5.19), defines the force functions, and the stepping probabilities associated with them, in accordance with eqn (5.6) and (5.7). The program in Figure 5.19 also incorporates an example of a conditional hyperbolic boundary, similar to the shape of an electrospinning jet (see Section 5.4). When the random walk hits the boundary, a strong force is applied on the monomer in the direction opposite to the direction of the last step.

$$
\begin{aligned}
P(z,\rho,\varphi) = \;& f \leftarrow \begin{pmatrix} Az_0 + Az_1 \cdot z + Az_2 \cdot z^2 \\ A\rho_0 + A\rho_1 \cdot \rho + A\rho_2 \cdot \rho \cdot z \\ A\varphi_0 + A\varphi_1 \cdot \varphi + A\varphi_2 \cdot \varphi \cdot z \end{pmatrix} && \text{Force functions (quadratic example)} \\
& f \leftarrow f - 10^{10} \cdot \begin{pmatrix} 0 \\ \operatorname{sign}(\rho) \\ \operatorname{sign}(\varphi) \end{pmatrix} \text{ if } \left(\rho^2 + \varphi^2\right) > \frac{r_0}{1 + k \cdot z} && \text{Forces on boundary (hyperbolic example)} \\
& Q \leftarrow 2 \cdot \sum_{x=0}^{2} \cosh\left(f_x\right) && \text{Partition function} \\
& P \leftarrow \frac{1}{Q} \cdot \exp\left[\begin{pmatrix} f_0 & -f_0 & f_1 & -f_1 & f_2 & -f_2 \end{pmatrix}^T\right] && \text{Stepping probabilities in 6 directions} \\
& \text{return } P
\end{aligned}
$$

Figure 5.19 Random walk stepping probability function in Mathcad. The function sets the force functions acting on each monomer at the given 3D position of the monomer [eqn (5.7)], and calculates the corresponding stepping probability for each of the 6 possible directions [eqn (5.6)]. The coordinates dimensions are in unit step. Also included is a hyperbolic boundary function that sets bouncing forces on the boundary in order to keep the random walk within a confined volume.

The trends of the stepping probabilities are demonstrated in Figure 5.20 for the simple case of an end force in the z direction [the term $A_{z,0}$ in eqn (5.7)], with all other forces null: when the force rises, the probability to step toward $+z$ increases, while the other probabilities decrease correspondingly. The probabilities in the presence of a boundary are demonstrated in the example of Figure 5.21, in which, when a boundary is hit while stepping in the $+\rho$ direction, the probability to step toward $-\rho$ jumps to 1, while the other probabilities drop to 0.

The random walk stepping function, $R(I, N)$ (Figure 5.22), executes random walks for a sample of I chains, each with N steps (*i.e.,* monomers). The function uses the stepping probabilities, calculated by the function $P(z, \rho, \varphi)$ for the next step, to partition the range 0–1 into divisions whose sizes are

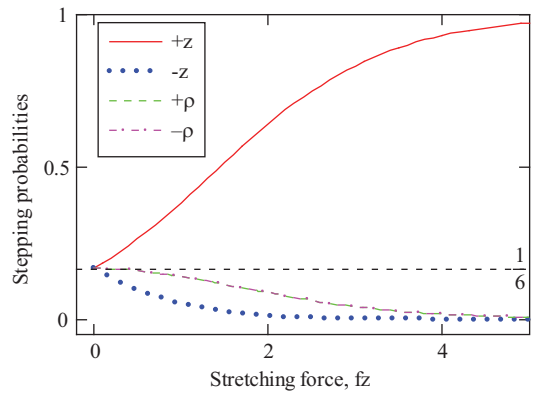

Figure 5.20 Stepping probabilities along the z axis, as a function of a stretching end force f_z.

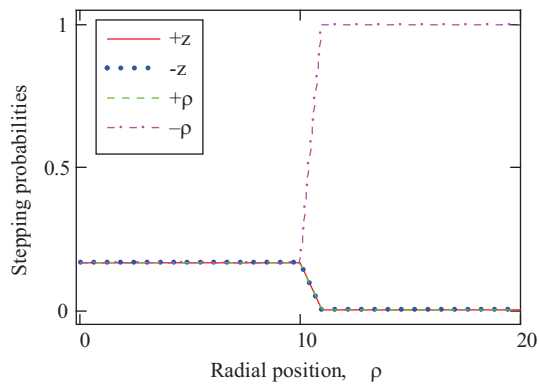

Figure 5.21 Stepping probabilities without forces, *versus* the radial position ρ, in the presence of a boundary parallel to z and located at $\rho = 10$.

```
R(I,N) = | for i ∈ 0..I                                          Sample loop, I times
         |   | (z_0)   (0)
         |   | (ρ_0) ← (0)                                      Coordinates initialization
         |   | (φ_0)   (0)
         |   for n ∈ 1..N                                       Chain loop, N times
         |     p_0 ← 0
         |     rndNum ← rnd(1)                                  Random number generation
         |     for j ∈ 0..5
         |       p_{j+1} ← P(z_{n-1}, ρ_{n-1}, φ_{n-1})_j + p_j   Probability bands
         |       q_j ← [(rndNum ≥ p_j) ∧ (rndNum < p_{j+1})]     Stepping decision
         |     (z_n)   (z_{n-1} + q_0 - q_1)
         |     (ρ_n) ← (ρ_{n-1} + q_2 - q_3)                    Stepping
         |     (φ_n)   (φ_{n-1} + q_4 - q_5)
         |   R_i ← (z ρ φ)^T                                    Chain i conformation
         | return R                                             All chains in sample
```

Figure 5.22 Random walk stepping function in Mathcad. The function runs random walks for a sample of I chains, each of N monomers, using the stepping probabilities calculated by the function P (Figure 5.19). The function returns the full position vectors of each chain and monomer in the sample. A random number between 0 and 1 is generated for each step, so that a direction with a higher probability will have a higher chance to be selected for stepping.

proportional to the probabilities. A random number, uniformly distributed between 0 and 1, is generated, and the division on which it falls is selected as the stepping direction.

The function $R(I, N)$ returns the full stepping history of all the chains in the sample. This data is used by other utilities (not presented here), to draw the 3D conformation of the stretched chains, to calculate the statistical distribution of the end-to-end distance R and the corresponding statistical moments, to calculate the orientational preference of chain segments, to calculate the free energy of chains, and more. Examples of chain conformations under stretching are shown in Figure 5.23, both without and with a cylindrical boundary (similar to the outer surface of a jet). Boundary causes widening of chains, though not significantly, in parallel to its surface (also observed in 1D theoretical analysis[30]).

The probability density of the end-to-end distance, $R = |\vec{R}|$ (Figure 5.24), shows that, in the case of a tensile force at chain ends, the distribution width remains essentially unchanged, except under very high forces where the distance is bounded by the fully extended length of the chain.

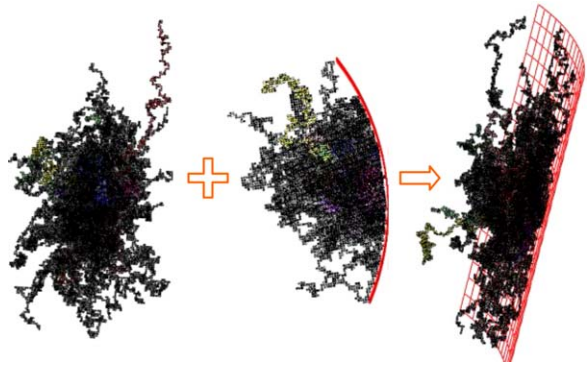

Figure 5.23 Example of random walk simulations of 100 freely-jointed chains, each with $N = 1000$ monomers. From left: chains under a field force $f_z = 0.004z$, free chains in the presence of a cylindrical boundary, and superposition of both.

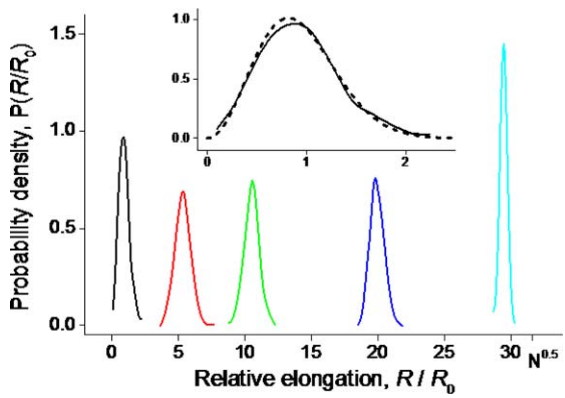

Figure 5.24 Probability density of relative end-to-end distances of 1000 simulated chains, each with $N = 1000$ monomers. A stretching end force f_z is applied, equal to (from left): 0, 0.5, 1, 2, and 4. A comparison to theory [dashed line, eqn (5.2)] is shown in the inset ($f_z = 0$).

5.6.2 Network Simulation Procedure

The simulation starts at an initial subchain, and proceeds from subchain to subchain in accordance with the procedure described in Figure 5.25 (additional details are provided in ref. 11). The force at a given position is calculated by eqn (5.23) or, alternatively, by adding the force increment from eqn (5.20) to the force in the previous subchain. The mesh size is then obtained by running a RW for the current subchain. In the axial direction, the simulation typically runs a sequence of $\sim 10^6$ subchains. In the radial direction, the number of subchains is fixed, given by $r_0/\xi_0 \sim 10^4$, and the simulation starts at the network radius, given at each position z by eqn (5.27), and proceeds toward the jet center.

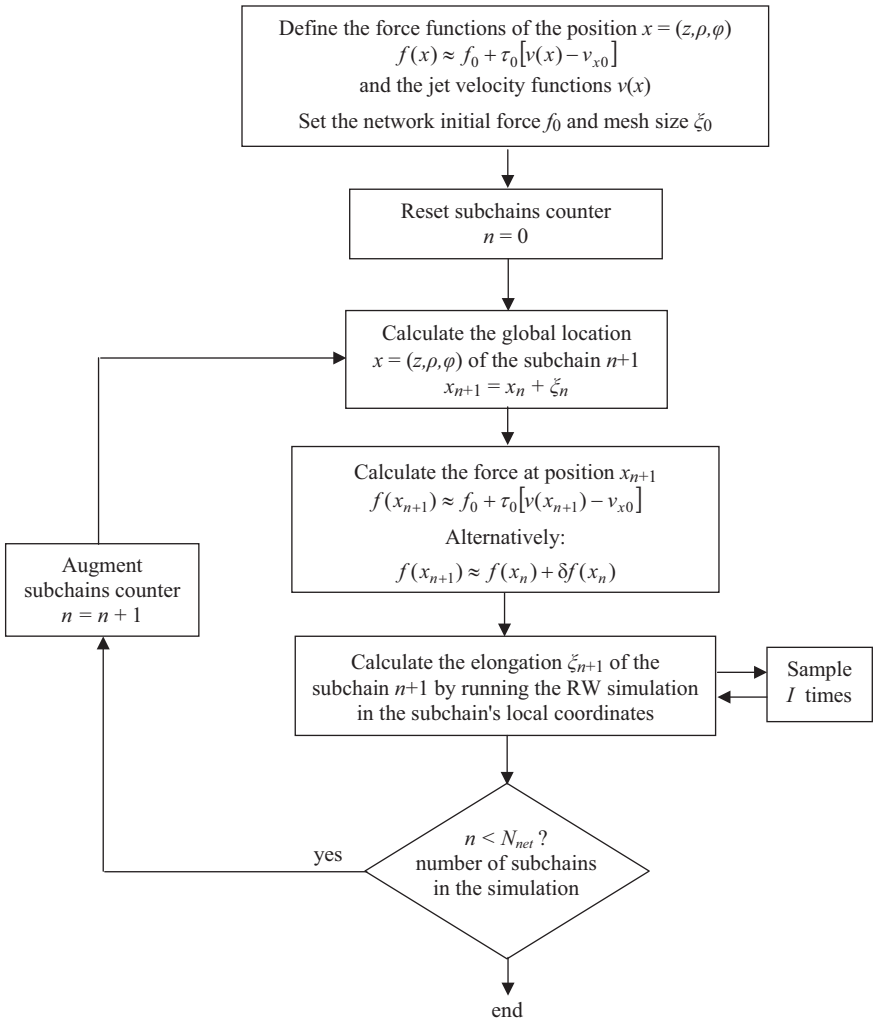

Figure 5.25 Procedure for RW simulation of a polymer network in an extensional flow.

Acknowledgements

The generous financial help of the Technion, the United States-Israel Binational Science Foundation, the RBNI-Russell Berrie Nanotechnology Institute, and the Israel Science Foundation is gratefully acknowledged. We thank Dr Arkadii Arinstein for insightful discussions on polymer dynamics.

References

1. T. Han, A. L. Yarin and D. H. Reneker, *Polymer*, 2008, **49**, 1651–1658.

2. P. Gupta, C. Elkins, T. E. Long and G. L. Wilkes, *Polymer*, 2005, **46**, 4799–4810.
3. D. H. Reneker, A. L. Yarin, E. Zussman and H. Xu, *Adv. Appl. Mech.*, 2007, **41**, 43–195.
4. D. H. Reneker, A. L. Yarin, H. Fong and S. Koombhongse, *J. Appl. Phys.*, 2000, **87**, 4531–4547.
5. L. M. Bellan, H. G. Craighead and J. P. Hinestroza, *J. Appl. Phys.*, 2007, **102**, 094308.
6. M. M. Hohman, M. Shin, G. Rutledge and M. P. Brenner, *Phys. Fluids*, 2001, **13**, 2201–2220.
7. Y. M. Shin, M. M. Hohman, M. P. Brenner and G. C. Rutledge, *Polymer*, 2001, **42**, 9955–9967.
8. M. Burman, A. Arinstein and E. Zussman, *Appl. Phys. Lett.*, 2008, **93**, 193118.
9. A. Arinstein, M. Burman, O. Gendelman and E. Zussman, *Nat. Nanotechnol.*, 2007, **2**, 59–62.
10. M. Burman, A. Arinstein and E. Zussman, *Europhys. Lett.*, 2011, **96**, 16006.
11. I. Greenfeld, A. Arinstein, K. Fezzaa, M. H. Rafailovich and E. Zussman, *Phys. Rev. E: Stat., Nonlinear, Soft Matter Phys.*, 2011, **84**, 041806.
12. E. Zussman and A. Arinstein, *J. Polym. Sci., Part B: Polym. Phys.*, 2011, **49**, 691–707.
13. X. M. Sui and H. D. Wagner, *Nano Lett.*, 2009, **9**, 1423–1426.
14. X. M. Sui, E. Wiesel and H. D. Wagner, *J. Nanosci. Nanotechnol.*, 2011, **11**, 7931–7936.
15. A. J. Guenthner, S. Khombhongse, W. X. Liu, P. Dayal, D. H. Reneker and T. Kyu, *Macromol. Theory Simul.*, 2006, **15**, 87–93.
16. P. Dayal and T. Kyu, *Phys. Fluids*, 2007, **19**, 107106.
17. P. Dayal, J. Liu, S. Kumar and T. Kyu, *Macromolecules*, 2007, **40**, 7689–7694.
18. S. Koombhongse, W. X. Liu and D. H. Reneker, *J. Polym. Sci., Part B: Polym. Phys.*, 2001, **39**, 2598–2606.
19. C. L. Casper, J. S. Stephens, N. G. Tassi, D. B. Chase and J. F. Rabolt, *Macromolecules*, 2004, **37**, 573–578.
20. I. Greenfeld, K. Fezzaa, M. H. Rafailovich and E. Zussman, *Macromolecules*, 2012, **45**, 3616–3626.
21. A. Camposeo, I. Greenfeld, F. Tantussi, S. Pagliara, M. Moffa, F. Fuso, M. Allegrini, E. Zussman and D. Pisignano, *Nano Lett.*, 2013, **13**, 5056–5062.
22. I. Greenfeld, Polymer network dynamics during electrospinning and its effect on the fibers nanostructure: Modeling, simulation and experiments, PhD thesis, Technion, Haifa, 2013.
23. M. Rubinstein and R. H. Colby, *Polymer physics*, Oxford University Press, Oxford; New York, 2003.
24. P. G. de Gennes, *Scaling concepts in polymer physics*, Cornell University Press, Ithaca, N.Y., 1979.

25. H. A. Kramers, *J. Chem. Phys.*, 1946, **14**, 415–424.
26. R. P. Feynman, *Statistical mechanics; a set of lectures*, W. A. Benjamin, Reading, Mass., 1972.
27. P. G. de Gennes, *J. Chem. Phys.*, 1974, **60**, 5030–5042.
28. I. Greenfeld and E. Zussman, *J. Polym. Sci., Part B: Polym. Phys.*, 2013, **51**, 1377–1391.
29. S. N. Reznik and E. Zussman, *Phys. Rev. E: Stat., Nonlinear, Soft Matter Phys.*, 2010, **81**, 026313.
30. I. Greenfeld, Effect of polymer matrix structure on mechanical properties of electrospun nanofibers, PhD research proposal, Technion, Haifa, 2009.